



FERMILAB-PUB-90/154-T

MAD/PH/577

August 1990

## Observability of a Heavy Higgs Boson at Hadron Supercolliders

U. Baur

*Physics Department, University of Wisconsin  
Madison, WI 53706, USA*

and

E. W. N. Glover

*Fermi National Accelerator Laboratory  
P. O. Box 500, Batavia, IL 60510, USA*

### ABSTRACT

We present a coherent analysis of Higgs boson production in the channels  $pp \rightarrow ZZX \rightarrow \ell^+ \ell^- \ell'^+ \ell'^- X$  ( $\ell, \ell' = e, \mu$ ) and  $pp \rightarrow ZZX \rightarrow \ell^+ \ell^- \nu \bar{\nu} X$  ( $\nu = \nu_e, \nu_\mu, \nu_\tau$ ) for  $m_H \geq 600$  GeV at hadron supercolliders, using the exact matrix elements for  $gg \rightarrow ZZ$  and  $qq \rightarrow qqZZ$ . The importance of a complete understanding of the shape of the perturbative  $pp \rightarrow ZZX$  background from non-resonant diagrams is emphasized. We find that the Higgs boson discovery potential of the LHC with  $10^5 \text{ pb}^{-1}$  is roughly equivalent to that of the SSC with  $10^4 \text{ pb}^{-1}$ . In particular, a Higgs boson with mass of up to 800 GeV can be identified at the LHC (SSC) with an integrated luminosity of  $10^5 \text{ pb}^{-1}$  ( $10^4 \text{ pb}^{-1}$ ). For  $m_H > 800$  GeV, a clear resonance structure is missing, however, one can still discriminate between a heavy Higgs boson with  $m_H \sim \mathcal{O}(1 \text{ TeV})$  and a light Higgs boson ( $m_H \lesssim 2M_Z$ ) at the SSC.



## 1. Introduction

One of the main goals of present and future accelerators is the search for the Higgs boson. Its discovery would constitute a significant confirmation of the standard model of electroweak interactions (SM). Current data from LEP experiments<sup>1)</sup> place a lower limit on the Higgs boson mass of  $m_H > \mathcal{O}(41 \text{ GeV})$ . Ultimately, LEP I experiments will be sensitive to Higgs boson masses up to  $\mathcal{O}(50 \text{ GeV})$ ,<sup>2)</sup> while at LEP II, one can search for a Higgs boson with mass up to at least 80 GeV in the reaction  $e^+e^- \rightarrow ZH$ .<sup>3)</sup>

For larger values of  $m_H$ , it is proposed to search for the Higgs boson at hadron supercolliders such as the LHC ( $pp$  collisions at  $\sqrt{s} = 16 \text{ TeV}$ ) or the SSC ( $pp$  collisions at  $\sqrt{s} = 40 \text{ TeV}$ ). Beneath the  $Z$  boson pair threshold,  $m_H < 2M_Z$ , the analysis is complicated by large QCD backgrounds which overwhelm the signal from the dominant  $H \rightarrow b\bar{b}$  decay. On the other hand, provided  $m_H > 2M_Z$ , the decay modes  $H \rightarrow ZZ \rightarrow \ell^+\ell^-\ell'^+\ell'^-$  ( $\ell, \ell' = e, \mu$ ) and  $H \rightarrow ZZ \rightarrow \ell^+\ell^-\nu\bar{\nu}$  ( $\nu = \nu_e, \nu_\mu, \nu_\tau$ ) both offer good opportunities to discover the Higgs boson. Decays into four charged leptons lead to a very clean signature, while  $H \rightarrow ZZ \rightarrow \ell^+\ell^-\nu\bar{\nu}$  results in a rather large number of events, due to the large  $Z \rightarrow \nu\bar{\nu}$  branching ratio.<sup>4)</sup>

The dominant production mechanism for Higgs bosons in the  $ZZ$  channel at hadron colliders are gluon fusion,<sup>5-7)</sup>

$$gg \rightarrow H \rightarrow ZZ, \quad (1.1)$$

where the gluons couple through a top quark loop to the Higgs boson, and vector boson fusion,<sup>8-10)</sup>

$$qq \rightarrow qqH \rightarrow qqZZ, \quad (1.2)$$

where the initial quarks or antiquarks each radiate a  $W$  or  $Z$  boson which then annihilate into a Higgs boson. The cross section of the gluon fusion process (1.1) depends strongly on the unknown top quark mass,  $m_t$ . Present data<sup>11)</sup> require  $m_t > 89 \text{ GeV}$ , which indicates that the gluon fusion process dominates at the SSC

provided  $m_H \lesssim 600$  GeV. On the other hand, the vector boson fusion process (1.2) contributes substantially to the total Higgs boson production cross section for larger Higgs boson masses.

Analytic expressions for the  $gg \rightarrow ZZ$  and  $qq \rightarrow qqZZ$  matrix elements, which include all contributions from non-resonant Feynman diagrams, have recently been presented in Ref. 7 and 12. In this paper, we use these matrix elements to make a coherent analysis of Higgs boson production in the  $pp \rightarrow ZZX \rightarrow \ell^+\ell^-\ell'^+\ell'^-X$  and  $pp \rightarrow ZZX \rightarrow \ell^+\ell^-\nu\bar{\nu}X$  channels at hadron supercolliders. In Section 2, we present results for the  $Z$  boson pair invariant mass distribution and the  $ZZ$  transverse mass spectrum by combining the cross sections from  $q\bar{q} \rightarrow ZZ$ ,  $gg \rightarrow ZZ$  and  $qq \rightarrow qqZZ$ . We show that a full understanding of the shape of the perturbative  $pp \rightarrow ZZX$  background from non-resonant diagrams is crucial in order to successfully search for a heavy Higgs boson (or any other strongly interacting scalar sector) at the LHC and SSC. We also demonstrate that the hadron calorimeter of a LHC (SSC) experiment must cover at least the rapidity range of  $|\eta| < 4$  (4.5) so that the  $H \rightarrow ZZ \rightarrow \ell^+\ell^-\nu\bar{\nu}$  signal is not completely overwhelmed by the  $Z + n$  jet,  $n \geq 1$ , ‘fake’ background. This fake background arises when jets accompanying a  $Z$  boson have rapidities outside the range covered by the calorimeter, and thus contribute to the missing transverse momentum of the event.

In Section 3, we use the results of the previous Section to study in detail the observability of a Higgs boson with mass  $m_H \geq 600$  GeV at both the LHC and SSC. We find that, for an integrated luminosity of  $10^4$  pb $^{-1}$ , the Higgs boson can be identified in the  $H \rightarrow ZZ \rightarrow \ell^+\ell^-\ell'^+\ell'^-$  channel at the LHC for  $m_H \lesssim 600$  GeV. The discovery potential of the LHC can be extended to  $m_H \lesssim 800$  GeV by either increasing statistics by a factor of 10 or by searching in the  $H \rightarrow ZZ \rightarrow \ell^+\ell^-\nu\bar{\nu}$  channel. Due to the higher center of mass energy, the SSC will be able to observe 800 GeV Higgs bosons with an integrated luminosity of only  $10^4$  pb $^{-1}$ . If the Higgs boson is heavier than about 800 GeV, a clear resonance structure no longer exists. In this case, the larger energy available at the SSC may still allow one to clearly separate a strongly interacting Higgs sector from a weakly interacting sector with  $m_H < 2M_Z$ , while this will be more difficult at the LHC, even with an integrated luminosity of  $10^5$  pb $^{-1}$ . Finally, we present our conclusions in Section 4.

## 2. Cross Sections

To compute the cross section for the inclusive reaction  $pp \rightarrow ZZX$  we use the lowest order matrix elements for  $q\bar{q} \rightarrow ZZ$ ,<sup>13)</sup>  $gg \rightarrow ZZ$ ,<sup>7)</sup> and  $qq \rightarrow qqZZ$ .<sup>12)</sup> LHC and SSC experiments are expected to cover an electron and muon rapidity range of  $|y_\ell| < 3$ . Since about 80% of the charged leptons originating from  $Z$  boson decays have rapidities in the range  $|y_Z - y_\ell| < 0.5$ , we approximately simulate the finite lepton coverage of future hadron supercollider experiments, with a rapidity cut on  $Z$  bosons decaying into a charged lepton pair of,

$$|y_Z| < 2.5. \quad (2.1)$$

For the two jets in  $qq \rightarrow qqZZ$  we require a separation in the rapidity-azimuthal-angle plane of,

$$\Delta R_{jj} = \left[ (\Delta\phi)_{jj}^2 + (\Delta\eta)_{jj}^2 \right]^{1/2} > 0.7. \quad (2.2)$$

This cut is necessary to achieve a finite cross section, due to the collinear singularity introduced by photon bremsstrahlung diagrams which are incorporated in our calculation, and has only a small effect on the total  $qq \rightarrow qqZZ$  cross section.<sup>12)</sup>

If both  $Z$  bosons decay into charged leptons, the invariant mass,  $m_{ZZ}$ , of the  $Z$  pair can be reconstructed and the most obvious strategy to search for the Higgs boson is to look for a resonance structure in the  $m_{ZZ}$  spectrum. For large Higgs boson masses, however, the Higgs width  $\Gamma_H$ , which grows like  $m_H^3/M_W^2$ , becomes very large and the resonance peak is significantly diluted. In this case, the signal to background ratio can be improved by imposing a cut,<sup>7,14)</sup>

$$p_{TZ} > \frac{1}{4} m_{ZZ}, \quad (2.3)$$

on the transverse momentum,  $p_{TZ}$ , of the  $Z$  bosons. Since the Higgs boson decays isotropically in its center of mass frame, one expects to observe a Jacobian peak at  $p_{TZ} \approx \frac{1}{2} \sqrt{m_H^2 - 4M_Z^2}$ . The background, on the other hand, is peaked at low transverse momentum.

Figure 1 shows the  $ZZ$  invariant mass spectrum,  $B \cdot d\sigma/dm_{ZZ}$ , for  $pp \rightarrow ZZ X \rightarrow \ell^+ \ell^- \ell'^+ \ell'^- X$  and various Higgs boson masses at the LHC and SSC. The factor  $B = 4.4 \cdot 10^{-3}$  represents the branching ratio for both  $Z$  bosons to decay into electrons or muons. One observes that the Higgs resonance structure is considerably more pronounced at the SSC than at the LHC. This is mostly due to the  $q\bar{q} \rightarrow ZZ$  background which is relatively more important at the LHC than at the SSC. Furthermore, the  $m_{ZZ}$  spectrum falls somewhat faster at the LHC, and cross sections at  $\sqrt{s} = 16$  TeV are typically a factor 4 – 10 smaller than at SSC energies.

While a reasonably clear resonance peak emerges for  $m_H \leq 800$  GeV, this is no longer the case for a Higgs boson with mass of the order of 1 TeV. In this case, the large width of the Higgs boson ( $\Gamma_H \approx 500$  GeV) dilutes the peak and spreads the signal over a large  $m_{ZZ}$  range. As a result, the signal of such a ‘very heavy’ Higgs boson constitutes of a rather flat enhancement of the  $m_{ZZ}$  distribution over the perturbative non-resonant background, represented by the solid line labeled  $m_H = 0$  GeV in Fig. 1. The perturbative non-resonant background is obtained by evaluating the  $gg \rightarrow ZZ$  and  $qq \rightarrow qqZZ$  matrix elements with  $m_H \sim 0$ . In this case, the unitarity violating contributions between Higgs and non-Higgs graphs completely cancel and the resulting  $m_{ZZ}$  distribution respects unitarity. In practice, the precise value of  $m_H$  is unimportant provided  $m_H < 2M_Z$ .

The SM parameters used in Fig. 1 and all subsequent figures are  $m_t = 120$  GeV,  $\alpha = \alpha(M_Z) = 1/128$ ,  $M_Z = 91.1$  GeV,  $\sin^2 \theta_W = 0.23$  and  $M_W = M_Z \cos \theta_W = 80$  GeV. These values are consistent with recent measurements at SLC,<sup>15)</sup> LEP,<sup>16)</sup> and the Tevatron.<sup>17)</sup> Since in all cases, we are probing the hadron structure functions at relatively large  $x$  ( $\geq 5 \cdot 10^{-3}$ ), there is little dependence on the choice of input parton distributions. We use the parameterisation of Duke and Owens, set I<sup>18)</sup> evaluated at momentum scale  $Q^2 = \hat{s}/4$ , where  $\hat{s}$  is the parton center of mass energy squared. The  $\mathcal{O}(\alpha_s^2)$  gluon fusion process is, in principle, sensitive to the choice of scale of the strong coupling constant, however, all scales,  $\hat{s}$ ,  $p_{TZ}^2 + M_Z^2$ ,  $m_H^2$  etc., are relatively large and different scale choices lead to changes of only  $\mathcal{O}(20\%)$ ; we choose  $Q^2 = \hat{s}/4$ .

The cross section of the gluon fusion process in the resonance region,  $m_H - \Gamma_H <$

$m_{ZZ} < m_H + \Gamma_H$ , depends significantly on the top quark mass. For  $m_t = 120$  GeV,  $gg \rightarrow ZZ$  is the most important source of 600 GeV Higgs bosons. With increasing  $m_H$ , the  $qq \rightarrow qqZZ$  subprocess gains in importance, and becomes competitive with gluon fusion at  $m_H \approx 1$  TeV. In the range of  $m_H$  we are considering,  $m_H \geq 600$  GeV, the  $gg \rightarrow ZZ$  cross section grows with  $m_t$  in the resonance region. For top quark masses less than 120 GeV, the contribution from gluon fusion is reduced leading to a slightly less pronounced resonance structure in  $d\sigma/dm_{ZZ}$ , particularly for smaller Higgs boson masses. On the other hand, if  $m_t$  is significantly larger than 120 GeV,  $gg \rightarrow ZZ$  would dominate Higgs boson production for all masses  $m_H$  up to  $\mathcal{O}(1 \text{ TeV})$ , resulting in a considerable enhancement of the Higgs boson peak in the  $m_{ZZ}$  distribution.

In Fig. 2, we show the total cross section  $B \cdot \sigma(m_{ZZ} > m_{\min})$  above a minimum invariant mass  $m_{\min}$  for  $pp \rightarrow ZZX \rightarrow \ell^+\ell^-\ell'^+\ell'^-X$  at the LHC and SSC as a function of  $m_{\min}$ . On the right vertical scale the expected number of events for an integrated luminosity of  $10^4 \text{ pb}^{-1}$  are indicated. A narrow Higgs boson resonance is characterized in  $B \cdot \sigma(m_{ZZ} > m_{\min})$  by a sharp drop in the cross section at  $m_{\min} = m_H$ . This is clearly demonstrated by the dotted line, which shows  $B \cdot \sigma(m_{ZZ} > m_{\min})$  for  $m_H = 600$  GeV. For larger Higgs boson masses the effect is somewhat washed out by the rapidly increasing width of the Higgs boson, however, the total cross section above a minimum invariant mass is still a rather sensitive indicator of the presence of a Higgs boson. The total cross section for  $m_{\min} \geq 1 \text{ TeV}$  is seen to be particularly sensitive to Higgs boson masses above 800 GeV, where the Higgs boson is strongly coupling.<sup>19)</sup> Experimentally,  $B \cdot \sigma(m_{ZZ} > m_{\min})$  has the advantage of representing data in an unbinned form which can conveniently be analyzed, *e.g.* by performing a Kolmogorov-Smirnov test. Furthermore, by calculating the difference of the total cross section for two values of  $m_{\min}$  one can easily obtain the  $pp \rightarrow ZZX \rightarrow \ell^+\ell^-\ell'^+\ell'^-X$  cross section for any arbitrary  $m_{ZZ}$  mass range.

A heavy Higgs boson with mass  $m_H > 800$  GeV does not lead to a pronounced resonance structure in  $d\sigma/dm_{ZZ}$ . Furthermore, the expected event rates at large values of the  $Z$  pair invariant mass are very small. Theoretical predictions for the perturbative non-resonant background must therefore be as accurate as possible

if one wants to discriminate a heavy Higgs boson from a light one with  $m_H < 2M_Z$ . In Fig. 3 we show the invariant mass distribution of the perturbative non-resonant  $pp \rightarrow ZZX \rightarrow \ell^+\ell^-\ell'^+\ell'^-X$  background (solid line) together with the contributions from the various subprocesses at the SSC. One observes that the dominant contribution to the background originates from  $q\bar{q} \rightarrow ZZ$ , with the  $gg \rightarrow ZZ$  subprocess being the second most important  $Z$  boson pair source at small values of  $m_{ZZ}$ . At large  $ZZ$  invariant masses, the  $qq \rightarrow qqZZ$  subprocess becomes more important than gluon fusion.

Combined, the  $gg \rightarrow ZZ$  and  $qq \rightarrow qqZZ$  cross sections represent a 35 – 60% (14 – 33%) correction to the  $q\bar{q} \rightarrow ZZ$  rate at the SSC (LHC). They are thus of the order of magnitude which one expects for the QCD corrections to  $q\bar{q} \rightarrow ZZ$ . These corrections have only been partially computed so far<sup>20)</sup> and, therefore, are not included in our calculation. The necessity of an accurate prediction of the perturbative non-resonant  $pp \rightarrow ZZX$  background, however, clearly warrants a calculation of the complete  $\mathcal{O}(\alpha_s)$  corrections to  $q\bar{q} \rightarrow ZZ$ .

We now turn to the reaction  $pp \rightarrow ZZX \rightarrow \ell^+\ell^-\nu\bar{\nu}X$ . Its primary advantage compared to  $pp \rightarrow ZZX \rightarrow \ell^+\ell^-\ell'^+\ell'^-X$  is the larger branching ratio of  $B = 0.026$  for  $ZZ \rightarrow \ell^+\ell^-\nu\bar{\nu}$ , which is, approximately, a factor 6 larger than that for  $ZZ \rightarrow \ell^+\ell^-\ell'^+\ell'^-$ . However, a price has to be paid for the increase in statistics. Since the neutrinos are only detected as missing transverse momentum,  $\not{p}_T$ , the  $ZZ$  invariant mass can no longer be reconstructed and one has to consider a transverse mass variable instead. Secondly, since real detectors do not cover the whole solid angle, potentially dangerous fake backgrounds arise from particles with a rapidity outside the range covered by the detector, and which, therefore, generate missing transverse momentum.

In our analysis of  $pp \rightarrow ZZX \rightarrow \ell^+\ell^-\nu\bar{\nu}X$ , we impose a rapidity cut of  $|y_Z| < 2.5$  (see Eq. (2.1)) on the  $Z$  which decays into the  $\ell^+\ell^-$  pair and the jet-jet separation cut (2.2) in the subprocess  $qq \rightarrow qqZZ$ . Furthermore, we require a missing  $p_T$  of,

$$\not{p}_T > 100 \text{ GeV}. \quad (2.4)$$

This missing  $p_T$  trigger helps reducing fake backgrounds where a non-zero  $\not{p}_T$  arises

from mismeasurements of momenta, e.g. due to cracks in the detector. Since the  $Z$  pair invariant mass cannot be reconstructed, the  $p_{TZ}$  cut (2.3) to enhance the Higgs boson signal cannot be applied in  $pp \rightarrow ZZX \rightarrow \ell^+\ell^-\nu\bar{\nu}X$ . The results of our calculations depend in principle on the jet rapidity coverage of the detector,  $|\eta_{\text{Had}}|$ , since jets in  $qq \rightarrow qqZZ$  with rapidity  $|\eta| > |\eta_{\text{Had}}|$  are treated as ‘missing’, and their momentum vector thus contributes to the missing transverse momentum vector.

Two different transverse mass variables are discussed in the literature. The two body transverse mass of the  $Z$  pair,<sup>21)</sup>

$$m_T^2(\mathbf{p}_{TZ}, \mathbf{\not{p}}_T) = \left[ (p_{TZ}^2 + M_Z^2)^{1/2} + (\not{p}_T^2 + M_Z^2)^{1/2} \right]^2 - (\mathbf{p}_{TZ} + \mathbf{\not{p}}_T)^2, \quad (2.5)$$

depends on the transverse momentum  $p_{TZ}$  of the reconstructed  $Z$  boson, as well as the missing transverse momentum  $\mathbf{\not{p}}_T$ . On the other hand, the  $ZZ$  transverse mass,<sup>4)</sup>

$$m_{TZZ} = 2(p_{TZ}^2 + M_Z^2)^{1/2}, \quad (2.6)$$

only involves the momentum of the  $Z$  boson which decays into  $\ell^+\ell^-$ , and is thus easier to handle experimentally. For  $Z$  bosons pairs with no transverse momentum,  $p_{TZZ} = 0$ ,  $m_T(\mathbf{p}_{TZ}, \mathbf{\not{p}}_T)$  and  $m_{TZZ}$  coincide. Away from the threshold region,  $m_{TZZ} \approx 2p_{TZ}$ , and the structure of the  $Z$  boson transverse momentum spectrum is directly reflected in the  $m_{TZZ}$  distribution.

In Fig. 4, we show the  $m_{TZZ}$  distribution,  $B \cdot d\sigma/dm_{TZZ}$ , at the LHC and SSC for various Higgs boson masses. For  $m_H \leq 800$  GeV, the Higgs boson peak, which is clearly visible in the  $m_{ZZ}$  distribution, is degraded to a broad shoulder. The effect of a heavy Higgs boson of mass  $m_H \sim \mathcal{O}(1 \text{ TeV})$  is a smooth, almost structureless, enhancement of the perturbative non-resonant background (solid line), particularly at the LHC. An accurate theoretical prediction of the background will therefore be very important in order to discriminate a heavy Higgs boson from a weakly interacting Higgs sector in this channel.

The long-dashed lines in Fig. 4 represent the background from  $pp \rightarrow ZjX \rightarrow \ell^+\ell^-jX$ . This fake background arises when the jet rapidity is outside the range

covered by the calorimeter of the detector, and thus contributes to the missing transverse momentum of the event.<sup>22)</sup> The three long-dashed lines give an estimate of this fake background for a calorimeter coverage of  $|\eta_{\text{Had}}| = 3, 4$  and  $4.5$  (3.5, 4.5 and 5) respectively, at the LHC (SSC), *i.e.* when jets with rapidity larger than this value are not identified. Additional, potentially important, contributions to this background arise from  $pp \rightarrow Z + n \text{ jet}$  with  $n \geq 2$ . However, these contributions cannot be reliably calculated at present with purely partonic Monte Carlos since existing calculations for  $Z + n \text{ jet}$  production<sup>23)</sup> do not take into account soft and virtual corrections. Jet transverse momentum and separation cuts are thus necessary to avoid infrared and collinear singularities and to achieve a finite cross section. If the jets are not observed, these cuts are meaningless and cannot be applied. The  $pp \rightarrow Z + n \text{ jet}$  contributions will, however, always enhance the  $Z\not{p}_TX$  background. The long-dashed lines in Fig. 4 can thus be viewed as a conservative *lower* bound on the fake  $Z\not{p}_TX$  background.

From Fig. 4, it is clear that LHC (SSC) detectors must have a hadron calorimeter covering the rapidity range  $|\eta| < 4$  (4.5) if one wants to search for the Higgs boson in  $pp \rightarrow ZZ X \rightarrow \ell^+ \ell^- \nu \bar{\nu} X$ . In certain cases, where an accurate determination of the perturbative non-resonant background at low values of  $m_{TZZ}$  is important, a coverage out to  $|\eta| = 4.5$  (5) may be required. Our results for the SSC agree qualitatively with those of Ref. 24.

As we have mentioned above, the  $m_{TZZ}$  distribution for  $qq \rightarrow qqZZ$  depends explicitly on the hadron calorimeter coverage of the detector. The results shown in Fig. 4 (solid, dashed, dotted and dash-dotted lines) have been obtained assuming that the range out to  $|\eta_{\text{Had}}| = 4$  (4.5) is covered at the LHC (SSC). The dependence of  $B \cdot d\sigma/dm_{TZZ}$  on the calorimeter coverage, however, is quite weak, and almost identical results are obtained *e.g.* for  $|\eta_{\text{Had}}| = 2.5$ . This is because the two quark jets in  $qq \rightarrow qqZZ$  typically have a transverse momentum of  $\mathcal{O}(50 - 100 \text{ GeV})$  which is much smaller than the missing  $p_T$  originating from  $Z \rightarrow \nu \bar{\nu}$ .

One might wonder whether the  $pp \rightarrow ZjX$  fake background can be reduced by imposing more stringent cuts. It turns out that this is not the case. For example, a rapidity cut of  $|y_Z| < 2$  instead of (2.1) reduces both signal and background

by approximately 20%, without changing the slope of the curves. Alternatively, a more stringent  $\cancel{p}_T$  cut merely increases the  $m_{TZZ}$  threshold for both signal and background, and leaves the distributions essentially unchanged at large  $m_{TZZ}$ .

There is an additional fake background from the production of  $b\bar{b}$ ,  $t\bar{t}$  and  $W^+W^-$  pairs, followed by decays into leptons, which can also give rise to a  $\ell^+\ell^-$  pair accompanied by missing transverse momentum. The size of this background depends on how well lepton pairs from  $Z$  decay can be distinguished from continuum production, which, in turn depends on the detector resolution. For the types of detectors under consideration for SSC and LHC experiments, the resolution is sufficiently good that the heavy quark background is reduced to a level far below the signal,<sup>24–26)</sup> and does not present a serious problem.

Results very similar to those shown in Fig. 4 are obtained for the  $m_T(p_{TZ}, \cancel{p}_T)$  distribution. This can be easily understood by noting that the  $q\bar{q} \rightarrow ZZ$  and  $gg \rightarrow ZZ$  subprocesses are the major contributions to the  $m_{TZZ}$  and  $m_T(p_{TZ}, \cancel{p}_T)$  distributions. In lowest order, the  $Z$  pair is produced with zero transverse momentum in these two reactions, and in this case, the two distributions coincide. Once higher order QCD corrections are taken into account, a non-zero  $p_{TZZ}$  is generated and the two transverse mass variables differ on an event by event basis. However, in the Higgs resonance region, the  $ZZ$  transverse momentum is usually much smaller than the individual  $Z$  boson  $p_T$ , so that the differences between the  $m_{TZZ}$  and  $m_T(p_{TZ}, \cancel{p}_T)$  distributions are small in this region. As a further consequence, the transverse momenta of the observed  $Z$  boson and the missing  $p_T$  tend to balance each other so that the  $m_{TZZ}$ ,  $p_{TZ}$  and  $\cancel{p}_T$  distributions are all very similar in this region.

One can also study the total cross section above a minimum transverse mass,  $B \cdot \sigma(m_{TZZ} > m_{T\min})$ . The resulting distributions are very similar to those shown in Fig. 2 and thus are not shown.

As we have already emphasized, an accurate prediction of the perturbative non-resonant background will be very important in distinguishing a heavy Higgs boson from a light one. In Fig. 5, we show the  $m_{TZZ}$  distribution of the  $pp \rightarrow ZZ X \rightarrow \ell^+\ell^-\nu\bar{\nu}X$  background (solid line) together with the contributions from

the various subprocesses at the SSC. As for the  $m_{ZZ}$  distribution (see Fig. 3), the major part of the background originates from  $q\bar{q} \rightarrow ZZ$  and  $gg \rightarrow ZZ$ . The  $qq \rightarrow qqZZ$  subprocess is, however, generally more important than it is in  $B \cdot d\sigma/dm_{ZZ}$ , particularly at large values of  $m_{TZZ}$ . Combined, the  $gg \rightarrow ZZ$  and  $qq \rightarrow qqZZ$  cross sections represent a 60 – 65% ( $\sim 30\%$ ) correction to the  $q\bar{q} \rightarrow ZZ$  rate at the SSC (LHC).

### 3. Higgs Boson Discovery Potential of the LHC and SSC

To further illustrate the points discussed above, we show in Fig. 6 and 7 the expected number of  $pp \rightarrow ZZX \rightarrow \ell^+\ell^-\ell'^+\ell'^-X$  and  $pp \rightarrow ZZX \rightarrow \ell^+\ell^-\nu\bar{\nu}X$  events versus  $m_{ZZ}$  and  $m_{TZZ}$ , for various Higgs boson masses, at the LHC and SSC. The size of the  $m_{ZZ}$  and  $m_{TZZ}$  bins is 40 GeV. ‘Data’ points show the Higgs boson signal with statistical errors, while the solid curves represent the perturbative non-resonant background. To transfer cross sections into event rates we choose two representative luminosities. Firstly, we take  $\int \mathcal{L} dt = 10^4 \text{ pb}^{-1}$  (lower points and curve), which corresponds to one ‘year’ of operation at  $10^{33} \text{ cm}^{-2}\text{s}^{-1}$ . Secondly, to show the effect of either a higher luminosity or several years of operation, we choose  $\int \mathcal{L} dt = 10^5 \text{ pb}^{-1}$  (upper points and curve), corresponding to one ‘year’ at  $10^{34} \text{ cm}^{-2}\text{s}^{-1}$  or ten ‘years’ at  $10^{33} \text{ cm}^{-2}\text{s}^{-1}$ . As before, we use  $m_t = 120 \text{ GeV}$  and the cuts specified in Eqs. (2.1) – (2.4), and make the additional assumption of a lepton identification efficiency of 100%.

From Fig. 6, it is clear that one should be able to discover a 600 GeV Higgs boson in the  $H \rightarrow ZZ \rightarrow \ell^+\ell^-\ell'^+\ell'^-$  channel at the LHC with  $10^4 \text{ pb}^{-1}$  provided  $m_t \geq 120 \text{ GeV}$ . However, for a top quark mass close to its present lower limit,  $m_t \approx 90 \text{ GeV}$ ,<sup>11)</sup> the signal of a Higgs boson with  $m_H = 600 \text{ GeV}$  only corresponds to a deviation from the perturbative background at the 98% confidence level.\* In this case, the value  $m_H \sim 600 \text{ GeV}$  seems to mark the Higgs boson discovery limit for the LHC in  $pp \rightarrow ZZX \rightarrow \ell^+\ell^-\ell'^+\ell'^-X$  with  $\int \mathcal{L} dt = 10^4 \text{ pb}^{-1}$ .

---

\* We use a standard  $\chi^2$  fit, where, in order to achieve sufficient events in each bin, all events with  $m_{ZZ} > 500 \text{ GeV}$  have been collected into a single bin. This procedure guarantees that a high confidence level cannot arise from a single event at high invariant mass.

It is also evident that an 800 GeV Higgs boson cannot be identified via a resonance structure in the four charged lepton mode with only  $10^4 \text{ pb}^{-1}$  at the LHC and  $m_t \leq 120 \text{ GeV}$ , simply because too few events are produced in the resonance region to make the signal observable. If the top quark mass is significantly larger than 120 GeV, one may, in fact, see a slight enhancement around  $m_{ZZ} = 800 \text{ GeV}$ , but even for a 200 GeV top quark, the Higgs resonance peak is not fully visible. On the other hand, provided the fake backgrounds can be controlled, the  $m_{TZZ}$  distribution points more directly at the presence of the Higgs boson, and, even if  $m_t = 90 \text{ GeV}$ , a deviation from the background is observable at the 97% confidence level. Due to the relatively large width of a 800 GeV Higgs boson ( $\Gamma_H \approx 260 \text{ GeV}$ ) it will not be easy to make a positive identification of such a scalar in the  $m_{TZZ}$  distribution. However, with  $10^5 \text{ pb}^{-1}$ , a clear resonance peak emerges in the four lepton channel for  $m_t \geq 90 \text{ GeV}$ , with at least  $\sim 10$  events per bin in the resonance region, and an 800 GeV Higgs boson can be discovered at the LHC.

If  $m_H > 800 \text{ GeV}$ , the signal is spread out over such a large range that it will be very difficult to see a significant deviation from the perturbative non-resonant background in either channel at the LHC. Even with  $10^5 \text{ pb}^{-1}$  one can, at best, hope to see a slight systematic increase of the cross section at large invariant masses for  $m_t \leq 120 \text{ GeV}$ .

In contrast to the situation at the LHC, a 800 GeV Higgs boson produces a rather clean signal in the  $m_{ZZ}$  spectrum at the SSC with  $10^4 \text{ pb}^{-1}$  (see Fig. 7). The size of the signal is approximately the same as for a Higgs boson with  $m_H = 600 \text{ GeV}$  at the LHC. However, due to the much reduced  $q\bar{q} \rightarrow ZZ$  background, the Higgs signal in the  $m_{TZZ}$  spectrum is much more pronounced than at the LHC. Furthermore, the prospects for observing a significant deviation from the perturbative non-resonant background for  $m_H > 800 \text{ GeV}$  are much better at the SSC. With an integrated luminosity of  $10^5 \text{ pb}^{-1}$ , one should be able to clearly discriminate between a heavy Higgs boson with mass  $m_H \sim \mathcal{O}(1 \text{ TeV})$  and a light Higgs boson ( $m_H < 2M_Z$ ) in the four charged lepton mode. For  $10^4 \text{ pb}^{-1}$ , this will only be possible in  $pp \rightarrow ZZX \rightarrow \ell^+\ell^-\nu\bar{\nu}X$ .

Figs. 6 and 7 clearly demonstrate that in order to observe a statistically signifi-

cant deviation from the perturbative non-resonant background for  $m_H > 800$  GeV, the shape and normalisation of the background curve must be known with a high degree of accuracy. This may not be as difficult as it seems for the following reasons. First, although both signal and background are subject to uncertainties in the structure functions and higher order corrections, the relative shapes of signal and background are less uncertain. Second, the normalisation will, in practice, be fixed by the data at small  $m_{ZZ}$  and  $m_{TZZ}$ .<sup>†</sup> An accurate measurement of the low mass region will be crucial in extracting any new physics since, in many cases, there is insufficient data at large  $m_{ZZ}$  and  $m_{TZZ}$  to assist in determining either the shape or normalisation.

Our discussion about the observability of a Higgs boson with mass  $m_H \geq 600$  GeV has been purely qualitative so far. It can be made somewhat more quantitative by extracting the maximum value  $S_{\max} \equiv S(M_{\min}) = \max\{S(m_{\min})\}$  of,

$$S(m_{\min}) = \left( \frac{[N_{m_H}(m_{\min}) - N_0(m_{\min})]^2}{N_0(m_{\min})} \right)^{1/2}, \quad (3.1)$$

where  $N_{m_H}(m_{\min})$  is the number of signal events for a Higgs boson of mass  $m_H$  with  $m_{ZZ} > m_{\min}$ , and  $N_0(m_{\min})$  the corresponding number of background events, in  $pp \rightarrow ZZ X \rightarrow \ell^+ \ell^- \ell'^+ \ell'^- X$ .  $N_{m_H}(m_{\min})$  and  $N_0(m_{\min})$  are obtained by multiplying  $B \cdot \sigma(m_{ZZ} > m_{\min})$  (see Fig. 2) with the integrated luminosity.  $M_{\min}$  is the value of  $m_{\min}$  which maximises  $S(m_{\min})$ .

$S_{\max}$  represents the statistical significance, in standard deviations, of the signal of a Higgs boson with mass  $m_H$ . For a narrow resonance,  $S_{\max}$  is equivalent to the significance of the cross section enhancement in the resonance region. By replacing  $N_0(m_{\min})$  in Eq. (3.1) by  $N_{m'_H}(m_{\min})$ ,  $S(m_{\min})$  can be generalized so that the corresponding value of  $S_{\max}$  gives a quantitative measure of how well a Higgs boson with mass  $m_H$  can be discriminated from a Higgs boson of mass  $m'_H$  at the LHC or SSC. This in turn reflects how well  $m_H$  can be measured in  $pp \rightarrow ZZ X \rightarrow \ell^+ \ell^- \ell'^+ \ell'^- X$ . A similar analysis can, in principle, be also carried out for  $H \rightarrow$

---

<sup>†</sup> As shown in Fig. 4, some of the small  $m_{TZZ}$  data will be contaminated by the fake  $Z + n$  jet background, rendering the overall normalisation more uncertain.

$ZZ \rightarrow \ell^+\ell^-\nu\bar{\nu}X$ . However, due to the  $Z + n$  jet fake background, the expected systematic errors in this channel are significantly larger than for the decay into four charged leptons, rendering the results of such an analysis more uncertain, and we have not attempted it.

Table 1 lists  $S_{\max}$  and the corresponding value of  $M_{\min}$  for various Higgs boson masses  $m_H$  and  $m'_H$  at the LHC and SSC, for an integrated luminosity of  $10^4 \text{ pb}^{-1}$  ( $10^5 \text{ pb}^{-1}$ ).  $M_{\min}$ , in general, does not change very much when the center of mass energy is increased from 16 TeV to 40 TeV. Furthermore, all values of  $M_{\min}$  are sufficiently small, so that the number of events is large enough to make this analysis meaningful. From the values of the statistical significance shown in Table 1 one can conclude that *the Higgs boson discovery potential of the LHC with  $10^5 \text{ pb}^{-1}$  is roughly equivalent to that of the SSC with  $10^4 \text{ pb}^{-1}$ .*

At the LHC, and with an integrated luminosity of  $\int \mathcal{L} dt = 10^4 \text{ pb}^{-1}$ , a 600 GeV Higgs boson produces a  $4.3\sigma$  deviation from the perturbative non-resonant background in the  $H \rightarrow ZZ \rightarrow \ell^+\ell^-\ell'^+\ell'^-$  channel. On the other hand, it can only be discriminated from a Higgs boson with  $m_H = 800 \text{ GeV}$  (1 TeV) at the  $2.0\sigma$  ( $2.9\sigma$ ) level. In this case, the  $m_{ZZ}$  distribution itself may be a better mass discriminator.

In Fig. 6 we have seen that there are too few events to make an 800 GeV Higgs resonance observable at the LHC with  $\int \mathcal{L} dt = 10^4 \text{ pb}^{-1}$ . Nevertheless, since the signal is spread over a fairly large invariant mass range, the total cross section above a minimum invariant mass is significantly larger than the background cross section, and leads to a  $2.0\sigma$  effect for  $M_{\min} = 620 \text{ GeV}$ . Although an effect of this size certainly does not establish the existence of a Higgs boson, it demonstrates that  $S_{\max}$  is a rather sensitive indicator for such a particle. For  $m_t = 200 \text{ GeV}$ , the significance of the Higgs signal is increased to  $4.2\sigma$ . On the other hand, an 800 GeV Higgs boson clearly produces a strong signal at the SSC. However, since the width rapidly increases with  $m_H$ , it will be more difficult to distinguish it from a heavier Higgs boson than from a lighter scalar (see Table 1).

Finally, Table 1 clearly shows that for a really heavy Higgs boson with  $m_H \sim \mathcal{O}(1 \text{ TeV})$ , *the SSC offers much better prospects for observing a statistically significant deviation from the perturbative non-resonant background, and thus for sep-*

arating a strongly interacting scalar sector from a light, weakly interacting Higgs sector than the LHC.

The values listed in Table 1 have been derived by assuming a lepton identification efficiency of 100%, and without taking into account any systematic errors. Viewed from this point they are thus somewhat optimistic. On the other hand, there are more powerful statistical methods available than the one used above to analyse real experimental data, and they may easily allow one to discriminate more accurately between different values of  $m_H$ . The values of  $S_{\max}$  in Table 1 should therefore be regarded as semiquantitative estimates, illustrating the qualitative statements made above.

#### 4. Summary and Conclusions

In this paper, we have presented a coherent analysis of Higgs boson production in  $pp \rightarrow ZZ X \rightarrow \ell^+ \ell^- \ell'^+ \ell'^- X$  and  $pp \rightarrow ZZ X \rightarrow \ell^+ \ell^- \nu \bar{\nu} X$  at hadron supercolliders, using the exact matrix elements for  $gg \rightarrow ZZ$  and  $qq \rightarrow qqZZ$ . We have shown results for the invariant and transverse mass of the  $Z$  boson pair by combining the cross sections from  $q\bar{q} \rightarrow ZZ$ ,  $gg \rightarrow ZZ$  and  $qq \rightarrow qqZZ$ . Furthermore, we have demonstrated that an accurate theoretical prediction of the shape and normalisation of the perturbative non-resonant background will be crucial in extracting the Higgs signal, particularly for  $m_H > 800$  GeV, where a clear resonance structure no longer exists. Combined, the  $gg \rightarrow ZZ$  and  $qq \rightarrow qqZZ$  background cross sections are about the same size as one expects the QCD corrections to  $q\bar{q} \rightarrow ZZ$  to be. Since the perturbative non-resonant background also constitutes a lower limit on the  $pp \rightarrow ZZ X$  cross section, a calculation of the complete  $\mathcal{O}(\alpha_s)$  corrections to  $q\bar{q} \rightarrow ZZ$  is clearly warranted.

In the  $ZZ$  transverse mass distribution,  $m_{TZZ}$  (see Eq. (2.6)), the Higgs resonance peak is degraded to a broad shoulder. Away from the  $Z$  pair threshold, the  $m_{TZZ}$ ,  $p_{TZ}$ ,  $\not{p}_T$  and the two body transverse mass distribution,  $m_T(p_{TZ}, \not{p}_T)$  (see Eq. (2.5)), are all very similar. Furthermore, the dependence of the  $m_{TZZ}$  distribution on the rapidity range covered by the calorimeter of the detector is quite weak. However, in order to sufficiently suppress the  $pp \rightarrow ZjX \rightarrow \ell^+ \ell^- jX$  fake

background, LHC (SSC) detectors must have a hadron calorimeter covering the rapidity range  $|\eta| < 4$  (4.5) (see Fig. 4).

Based on these results, we have studied the observability of a Higgs boson with mass  $m_H \geq 600$  GeV at the LHC and SSC. We find that, for  $\int \mathcal{L} dt = 10^4$  pb $^{-1}$ , the Higgs boson can be identified at the LHC in the four charged lepton decay mode provided  $m_H \lesssim 600$  GeV. The range of accessible Higgs boson masses at the LHC can be extended to  $m_H \sim 800$  GeV by either searching in the  $H \rightarrow ZZ \rightarrow \ell^+ \ell^- \nu \bar{\nu}$  channel or by increasing the integrated luminosity to  $10^5$  pb $^{-1}$ . In contrast, a 800 GeV Higgs boson produces a clean signal in  $B \cdot d\sigma/dm_{ZZ}$  at the SSC with only  $10^4$  pb $^{-1}$ . Broadly speaking, the Higgs boson discovery potential of the LHC with  $10^5$  pb $^{-1}$  is equivalent to that of the SSC with  $10^4$  pb $^{-1}$ .

For  $m_H > 800$  GeV, where the signal, due to the large width of the Higgs boson, consists of a smooth, almost structureless, enhancement of the perturbative non-resonant background (see Figs. 1 and 4), the SSC has a much better chance of observing a statistically significant effect than the LHC. In fact, even if no resonance structure in  $Z$  pair production is observed at the SSC, one should be able to clearly discriminate between a heavy, strongly interacting symmetry breaking sector, and a light perturbative sector characterized by a light Higgs boson with mass  $m_H < 2M_Z$ , provided that the perturbative non-resonant background is known with sufficient accuracy.

Finally, the conclusions presented here are somewhat more optimistic than those of previous studies, particularly for the LHC.<sup>25,26)</sup> The reasons for this are twofold. Firstly, and most importantly, throughout this work, we have assumed a rather large value for the top quark mass,  $m_t = 120$  GeV, some way above the current lower bound,  $m_t > 89$  GeV. However, our conclusions are not significantly softened even if the top quark is just around the corner,  $m_t \approx 90 - 95$  GeV. On the other hand, if the top quark is heavier,  $m_t \sim 200$  GeV, the Higgs boson signal will become more pronounced. Secondly, we utilise the exact matrix elements for  $Z$  boson pair production, which contain some sizeable interference effects, especially for  $gg \rightarrow ZZ$ , and which increase the effective size of the signal.

## ACKNOWLEDGEMENTS

We would like to thank S. Errede, K. Einsweiler, D. Froidevaux, I. Hinchliffe, K. Meier, D. Morris, K. Sliwa and C. P. Yuan for useful discussions. This research was supported in part by the University of Wisconsin Research Committee with funds granted by the Wisconsin Alumni Research Foundation, and in part by the U. S. Department of Energy under contract DE-AC02-76ER00881.

## REFERENCES

1. D. Decamp *et al.* (ALEPH Collaboration), CERN-PPE/90-101 preprint (July 1990), CERN-EP/90-70 preprint (May 1990), Phys. Lett. **241B**, 141 (1990) and Phys. Lett. **236B**, 233 (1990);  
M. Z. Akrawy *et al.* (OPAL Collaboration), CERN-EP/90-100 preprint (July 1990) and Phys. Lett. **236B**, 224 (1990);  
P. Abreu *et al.* (DELPHI Collaboration), CERN-EP/90-44 preprint (April 1990);  
B. Adeva *et al.* (L3 Collaboration), L3-010 preprint (June 1990).
2. M. Drees *et al.*, in *Proceedings of the Workshop Z Physics at LEP 1*, CERN 89-08, Vol. 2, p. 58 (1989), and references therein.
3. See *e.g.* S. L. Wu *et al.* in *Proceedings of the ECFA Workshop on LEP200*, Volume II, Aachen, Germany, 29 September - 1 October 1986, CERN 87-08, p. 312 and references therein;  
Z. Kunszt and W. J. Stirling, Phys. Lett. **242B**, 507 (1990).
4. R. N. Cahn and M. S. Chanowitz, Phys. Rev. Lett. **56**, 1327 (1986).
5. H. Georgi, S. L. Glashow, M. E. Mahacek and D. V. Nanopoulos, Phys. Rev. Lett. **40**, 692 (1978).
6. D. A. Dicus, C. Kao and W. W. Repko, Phys. Rev. **D36**, 1570 (1987);
7. E. W. N. Glover and J. J. van der Bij, Phys. Lett. **219B**, 488 (1989), and Nucl. Phys. **B321**, 561 (1989).
8. R. N. Cahn and S. Dawson, Phys. Lett. **136B**, 196 (1984), Phys. Lett. **138B**, 464(E) (1984);  
S. Dawson, Nucl. Phys. **B249**, 42 (1984);  
G. L. Kane, W. W. Repko and W. B. Rolnick, Phys. Lett. **148B**, 367 (1984).
9. M. S. Chanowitz and M. K. Gaillard, Phys. Lett. **142B**, 85 (1984).
10. A. Abbasabadi and W. W. Repko, Nucl. Phys. **B292**, 461 (1987), and Phys. Rev. **D37**, 2668 (1988).

11. F. Abe *et al.* (CDF Collaboration), Phys. Rev. Lett. **64**, 142 (1990);  
 F. Abe *et al.* (CDF Collaboration), Phys. Rev. Lett. **64**, 147 (1990);  
 H. B. Jensen, talk given at the *Meeting of the American Physical Society*,  
 Washington DC, April 16 – 19, 1990.
12. U. Baur and E. W. N. Glover, FERMILAB-PUB-90/75-T, MAD/PH/562,  
 preprint (April 1990), to appear in Nucl. Phys. B.
13. R. W. Brown and K. O. Mikaelian, Phys. Rev. **D19**, 922 (1979).
14. V. Barger, T. Han and R. J. N. Phillips, Phys. Lett. **206B**, 339 (1988).
15. G. S. Abrams *et al.* (MARK II Collaboration), Phys. Rev. Lett. **63**, 724  
 (1989).
16. B. Adeva *et al.* (L3 Collaboration), Phys. Lett. **231B**, 509 (1989);  
 D. Decamp *et al.* (ALEPH Collaboration), Phys. Lett. **231B**, 519 (1989);  
 M. Z. Akrawy *et al.* (OPAL Collaboration), Phys. Lett. **231B**, 530 (1989);  
 P. Aarnio *et al.* (DELPHI Collaboration), Phys. Lett. **231B**, 539 (1989).
17. F. Abe *et al.* (CDF Collaboration), Phys. Rev. Lett. **63**, 720 (1989).
18. D. Duke and J. Owens, Phys. Rev. **D30**, 49 (1984).
19. M. S. Chanowitz and M. K. Gaillard, Nucl. Phys. **B261**, 379 (1985).
20. V. Barger, J. L. Lopez and W. Putikka, Int. J. Mod. Phys. **A3**, 2181 (1988);  
 U. Baur, E. W. N. Glover and J. J. van der Bij, Nucl. Phys. **B318**, 106  
 (1989).
21. V. Barger, T. Han and R. J. N. Phillips, Phys. Rev. **D36**, 295 (1987).
22. R. N. Cahn *et al.* in *Proceedings of the Workshop on Experiments, Detectors  
 and Experimental Areas for the SSC*, (1987) p. 20.
23. K. Hagiwara and D. Zeppenfeld, Nucl. Phys. **B313**, 560 (1988);  
 F. A. Berends, W. T. Giele and H. Kuijf, Nucl. Phys. **B321**, 39 (1989);  
 V. Barger, T. Han, J. Ohnemus and D. Zeppenfeld, Phys. Rev. Lett. **62**,  
 1971 (1989) and Phys. Rev. **D40**, 2888 (1989);  
 F. A. Berends, W. T. Giele, R. Kleiss, H. Kuijf and W. J. Stirling, Phys.  
 Lett. **224B**, 237 (1989).

24. R. M. Barnett and I. Hinchliffe, LBL-28773. SSC-SDE-29 preprint (March 1990).
25. D. Froidevaux and B. van Eijk, CERN 88-02 report (1988) ed. J. H. Mulvey, p. 73.
26. D. Froidevaux. in *Proceedings of the Workshop on Physics at Future Accelerators*, La Thuile (Italy) and Geneva (Switzerland), CERN 87-07 report (1987), ed. J. H. Mulvey. Vol. 1, p. 61.

TABLE 1

Statistical significance of the Higgs boson signal at the LHC and SSC in  $pp \rightarrow ZZX \rightarrow \ell^+\ell^-\ell'^+\ell'^-X$ , for  $m_t = 120$  GeV and an integrated luminosity of  $10^4$  pb $^{-1}$  ( $10^5$  pb $^{-1}$ ). Both  $Z$  bosons are required to have rapidity,  $|y_Z| < 2.5$ , and transverse momentum,  $p_{TZ} > \frac{1}{4}m_{ZZ}$ .  $S_{\max} \equiv S(M_{\min}) = \max\{S(m_{\min})\}$  represents the significance, in standard deviations, of a Higgs boson with mass  $m_H$  compared to the perturbative non-resonant background ( $m'_H = 0$ ), and compared to a Higgs boson with a different mass  $m'_H$ .  $M_{\min}$  is the value of  $m_{\min}$  for which  $S(m_{\min})$  (see Eq. (3.1)) is maximal.

$m_H$ [GeV]	$m'_H$ [GeV]	LHC		SSC	
		$M_{\min}$ [GeV]	$S_{\max}$	$M_{\min}$ [GeV]	$S_{\max}$
600	0	500	4.3 (13.4)	500	12.7 (40.0)
	800	460	2.0 (6.5)	420	4.9 (15.5)
	1000	460	2.9 (9.3)	460	7.4 (23.5)
800	0	620	2.0 (6.5)	620	7.0 (22.2)
	600	420	1.7 (5.4)	700	4.4 (13.9)
	1000	580	0.8 (2.5)	580	2.1 (6.7)
1000	0	700	1.1 (3.5)	700	4.4 (13.9)
	600	460	2.2 (7.1)	420	5.4 (17.1)
	800	580	0.7 (2.3)	540	1.9 (5.9)

## FIGURE CAPTIONS

1. Invariant mass distribution,  $B \cdot d\sigma/dm_{ZZ}$ , of the  $Z$  boson pair in  $pp \rightarrow ZZ X \rightarrow \ell^+ \ell^- \ell'^+ \ell'^- X$  at (a) the LHC and (b) the SSC, for  $m_H = 600$  GeV (dotted line),  $m_H = 800$  GeV (dashed line) and  $m_H = 1000$  GeV (dash-dotted line). The  $m_H = 0$  GeV curve (solid line) represents the perturbative non-resonant background. Both  $Z$  bosons are required to have rapidity,  $|y_Z| < 2.5$ , and transverse momentum,  $p_{TZ} > \frac{1}{4} m_{ZZ}$ .
2. Total cross section  $B \cdot \sigma(m_{ZZ} > m_{\min})$  above a minimum invariant mass,  $m_{\min}$ , for  $pp \rightarrow ZZ X \rightarrow \ell^+ \ell^- \ell'^+ \ell'^- X$  at (a) the LHC and (b) the SSC, for  $m_H = 600$  GeV (dotted line),  $m_H = 800$  GeV (dashed line) and  $m_H = 1000$  GeV (dash-dotted line). The  $m_H = 0$  GeV curve (solid line) represents the perturbative non-resonant background. Both  $Z$  bosons are required to have rapidity,  $|y_Z| < 2.5$ , and a transverse momentum,  $p_{TZ} > \frac{1}{4} m_{ZZ}$ .
3. Invariant mass distribution of the perturbative non-resonant  $pp \rightarrow ZZ X \rightarrow \ell^+ \ell^- \ell'^+ \ell'^- X$  background at the SSC. The dotted, dashed and dash-dotted lines show the contributions from  $qq \rightarrow qqZZ$ ,  $gg \rightarrow ZZ$  and  $q\bar{q} \rightarrow ZZ$ . The solid line gives the sum of the cross sections of the three subprocesses. Both  $Z$  bosons are required to have rapidity,  $|y_Z| < 2.5$ , and transverse momentum,  $p_{TZ} > \frac{1}{4} m_{ZZ}$ .
4.  $Z$  boson pair transverse mass distribution,  $B \cdot d\sigma/dm_{TZZ}$ , in  $pp \rightarrow ZZ X \rightarrow \ell^+ \ell^- \nu \bar{\nu} X$  at (a) the LHC and (b) the SSC, for  $m_H = 600$  GeV (dotted line),  $m_H = 800$  GeV (dashed line) and  $m_H = 1000$  GeV (dash-dotted line). The  $m_H = 0$  GeV curve (solid line) represents the perturbative non-resonant background. The long-dashed curves show the background from  $pp \rightarrow Zj X \rightarrow \ell^+ \ell^- j X$ , where the jet has rapidity  $|\eta| > |\eta_{\text{Had}}|$  and therefore ‘fakes’ missing transverse momentum, for various calorimeter coverages  $|\eta_{\text{Had}}|$ . In all cases a  $\not{p}_T > 100$  GeV cut and a rapidity cut of  $|y_Z| < 2.5$  on the  $Z$  decaying into  $\ell^+ \ell^-$  are imposed.
5.  $Z$  boson pair transverse mass distribution of the perturbative non-resonant  $pp \rightarrow ZZ X \rightarrow \ell^+ \ell^- \nu \bar{\nu} X$  background at the SSC. The dotted, dashed and

dash-dotted lines show the contributions from  $qq \rightarrow qqZZ$ ,  $gg \rightarrow ZZ$  and  $q\bar{q} \rightarrow ZZ$ . The solid line gives the sum of the cross sections of the three subprocesses. The  $Z$  boson decaying into  $\ell^+\ell^-$  is required to have rapidity  $|y_Z| < 2.5$ , and a  $p_T > 100$  GeV cut is imposed.

6. Expected event rates for  $pp \rightarrow ZZX \rightarrow \ell^+\ell^-\ell'^+\ell'^-X$  and  $pp \rightarrow ZZX \rightarrow \ell^+\ell^-\nu\bar{\nu}X$  as a function of  $m_{ZZ}$  and  $m_{TZZ}$  respectively for  $m_H = 600, 800$  and  $1000$  GeV at the LHC. ‘Data’ points show the Higgs boson signal in 40 GeV bins with statistical errors, while continuous curves represent the perturbative non-resonant background. Upper (lower) points and curves correspond to an integrated luminosity of  $10^5 \text{ pb}^{-1}$  ( $10^4 \text{ pb}^{-1}$ ). The cuts specified in Eqs. (2.1) – (2.4) are imposed.
7. Expected event rates for  $pp \rightarrow ZZX \rightarrow \ell^+\ell^-\ell'^+\ell'^-X$  and  $pp \rightarrow ZZX \rightarrow \ell^+\ell^-\nu\bar{\nu}X$  as a function of  $m_{ZZ}$  and  $m_{TZZ}$  respectively for  $m_H = 600, 800$  and  $1000$  GeV at the SSC. ‘Data’ points show the Higgs boson signal in 40 GeV bins with statistical errors, while continuous curves represent the perturbative non-resonant background. Upper (lower) points and curves correspond to an integrated luminosity of  $10^5 \text{ pb}^{-1}$  ( $10^4 \text{ pb}^{-1}$ ). The cuts specified in Eqs. (2.1) – (2.4) are imposed.

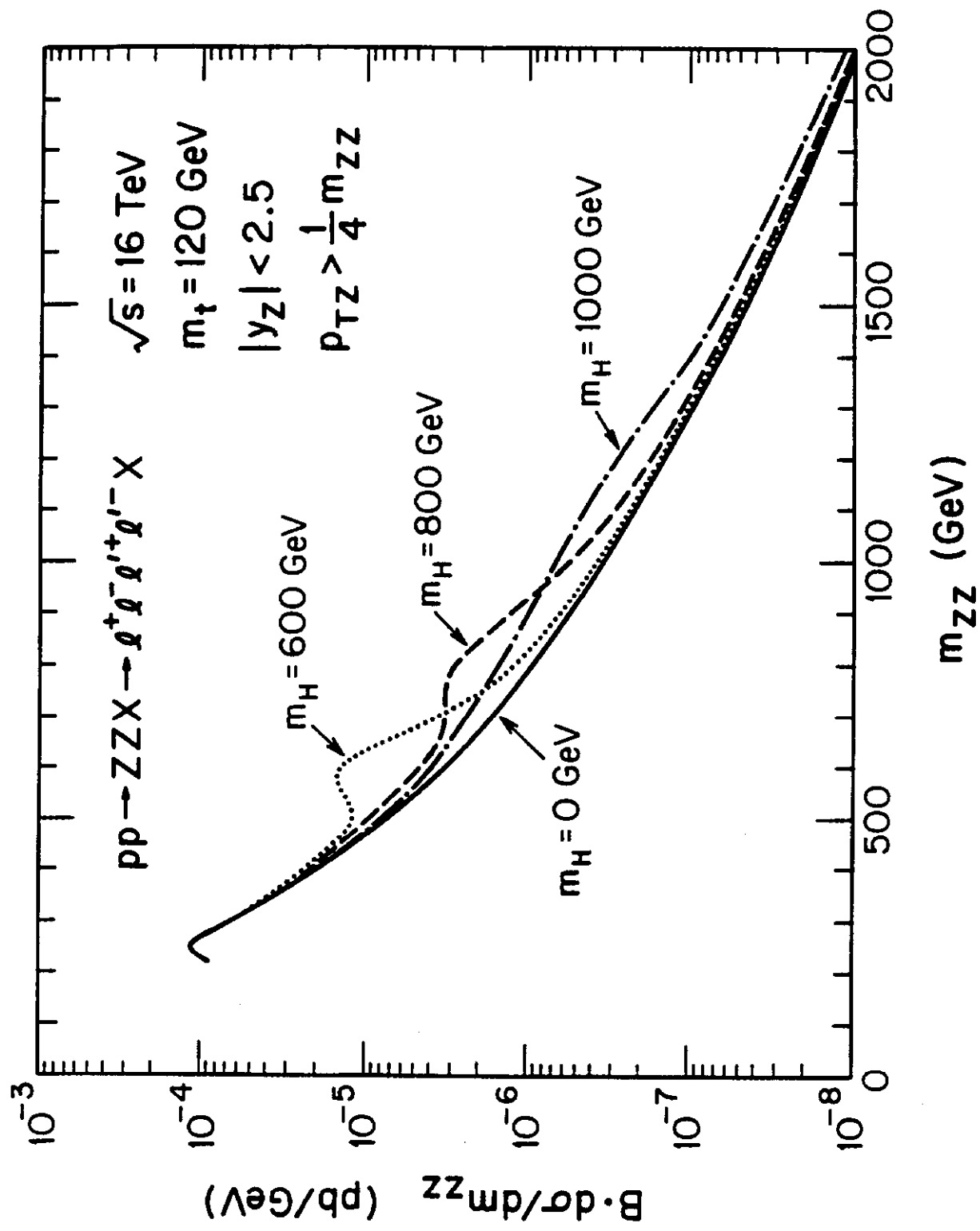


Fig. 1a

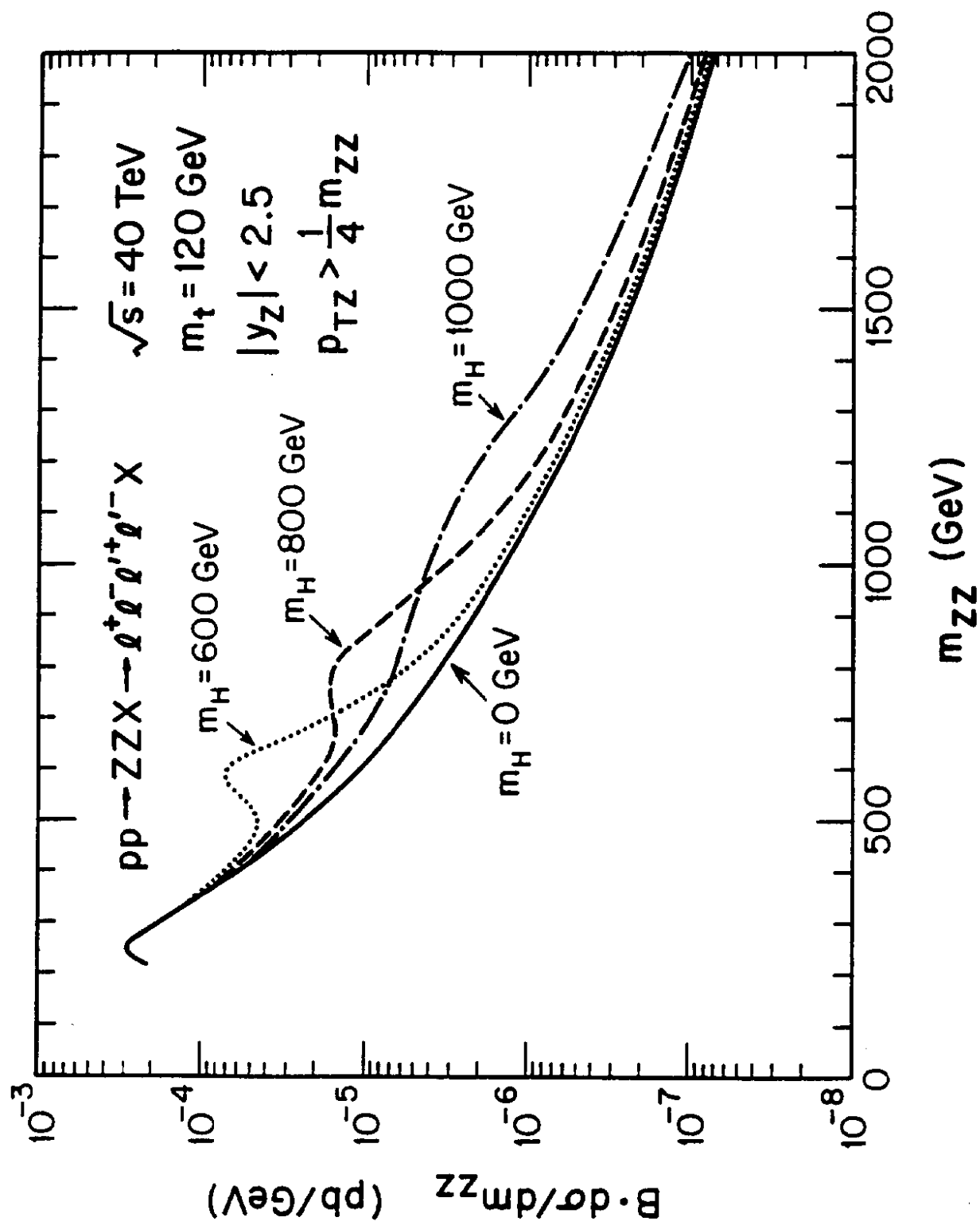


Fig. 1b

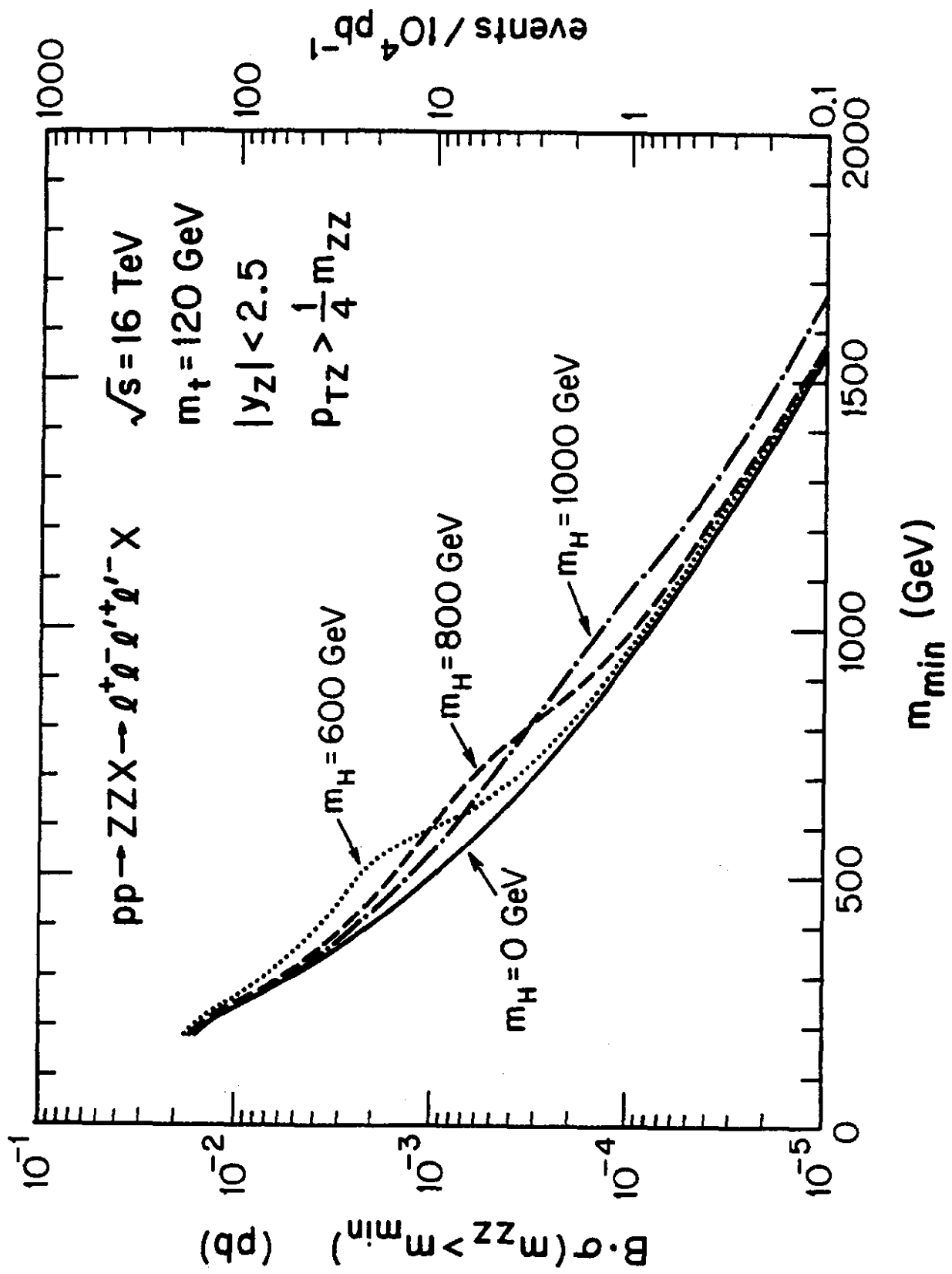


Fig. 2a

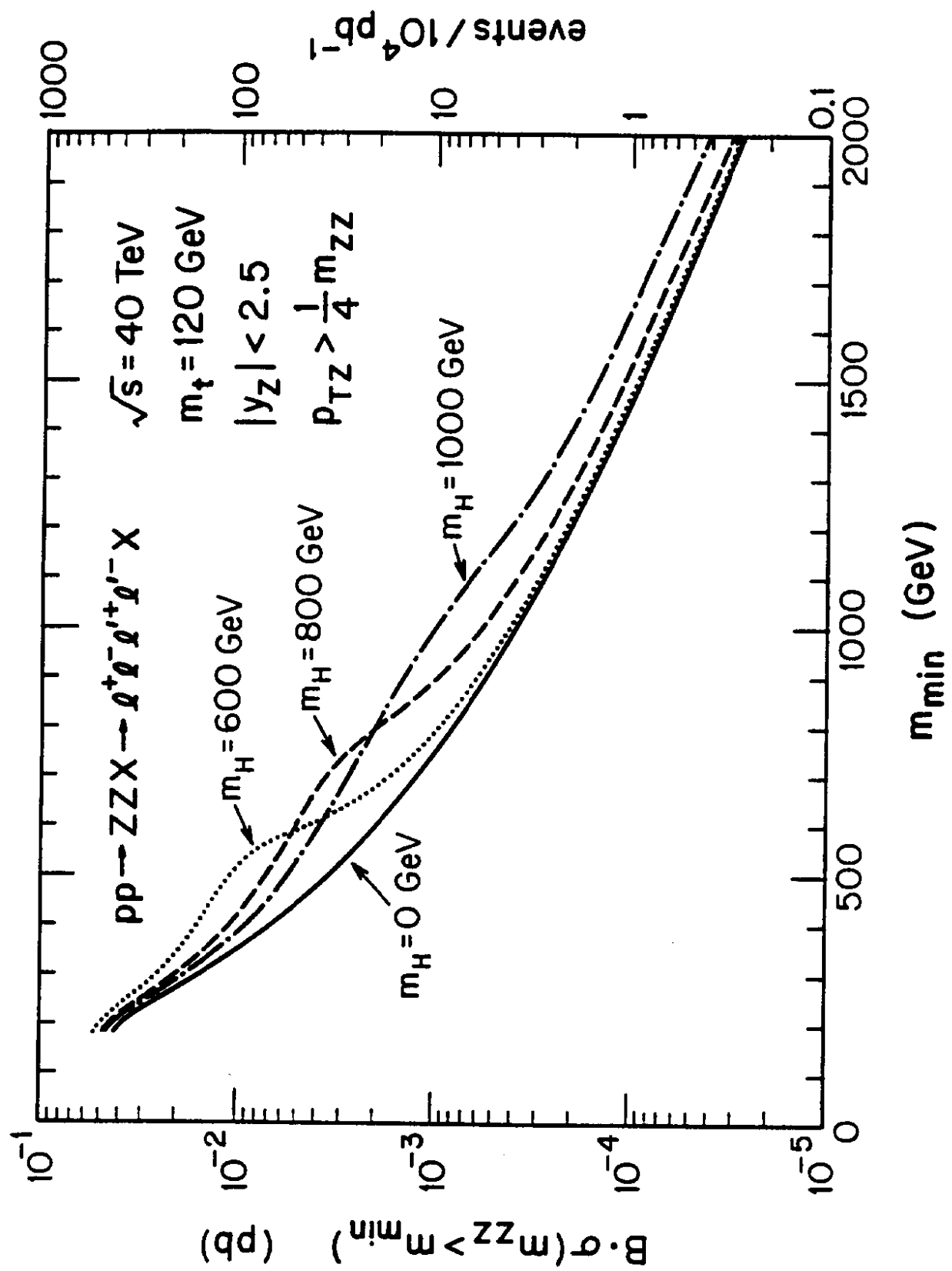


Fig. 2b

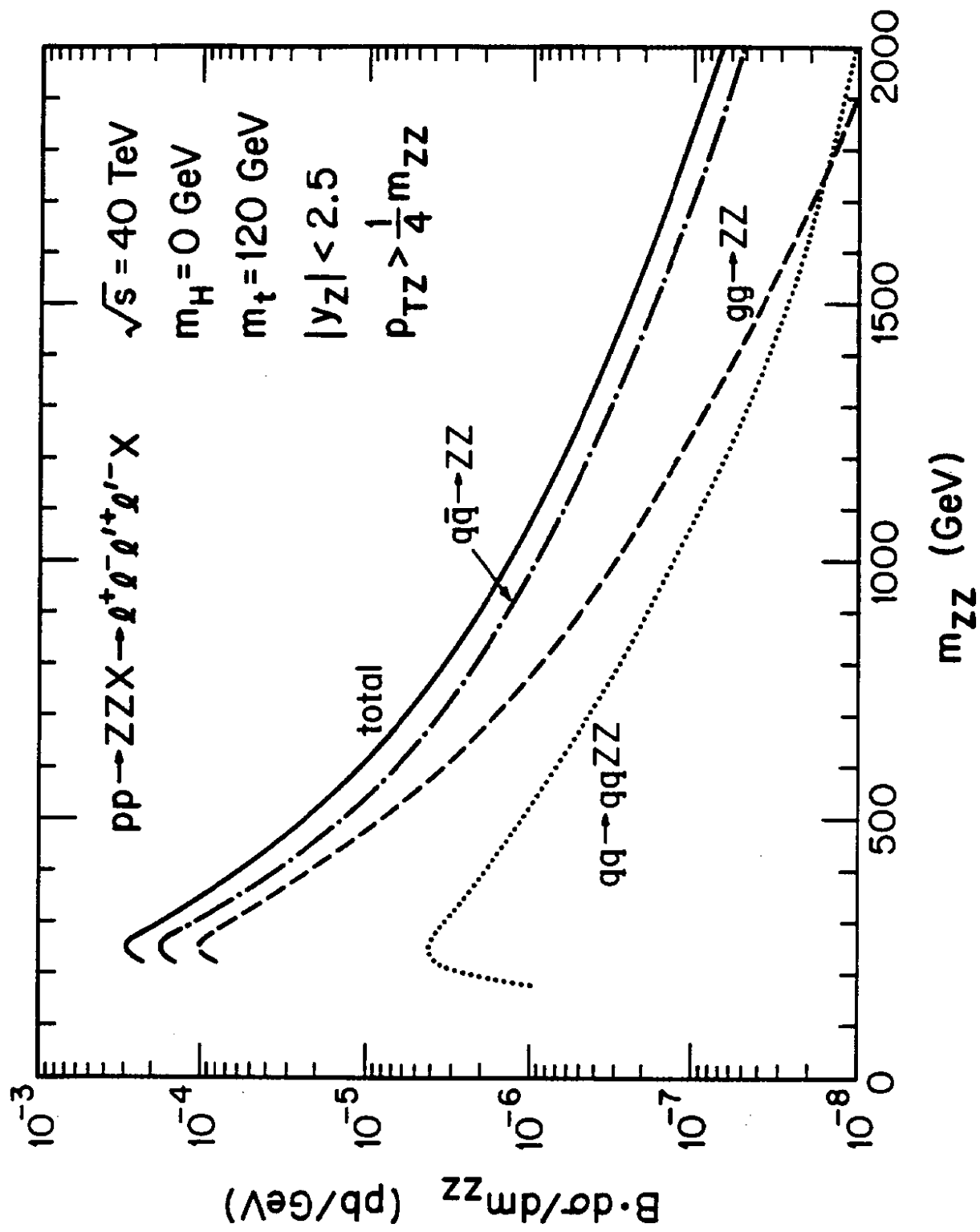


Fig. 3

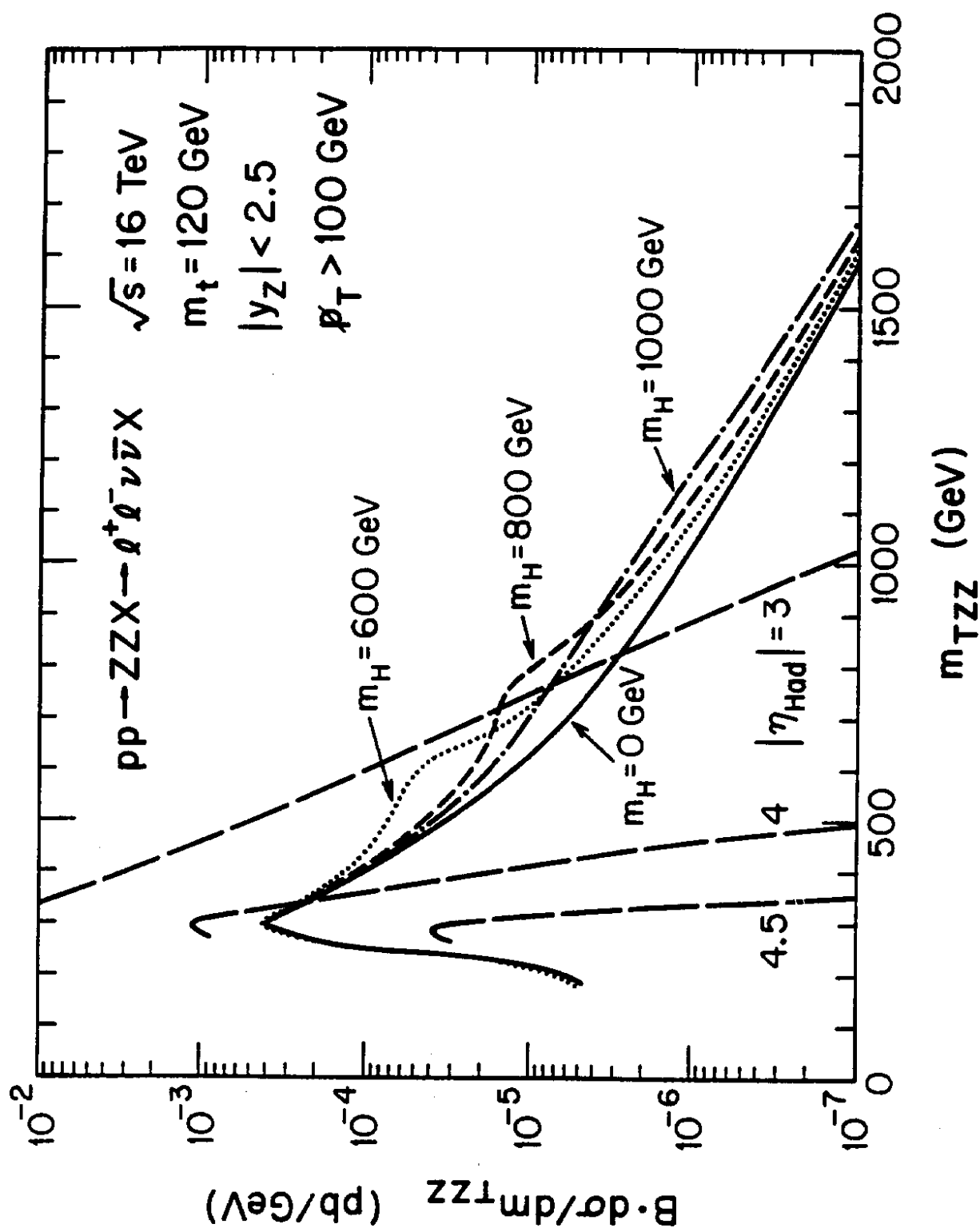


Fig. 4a

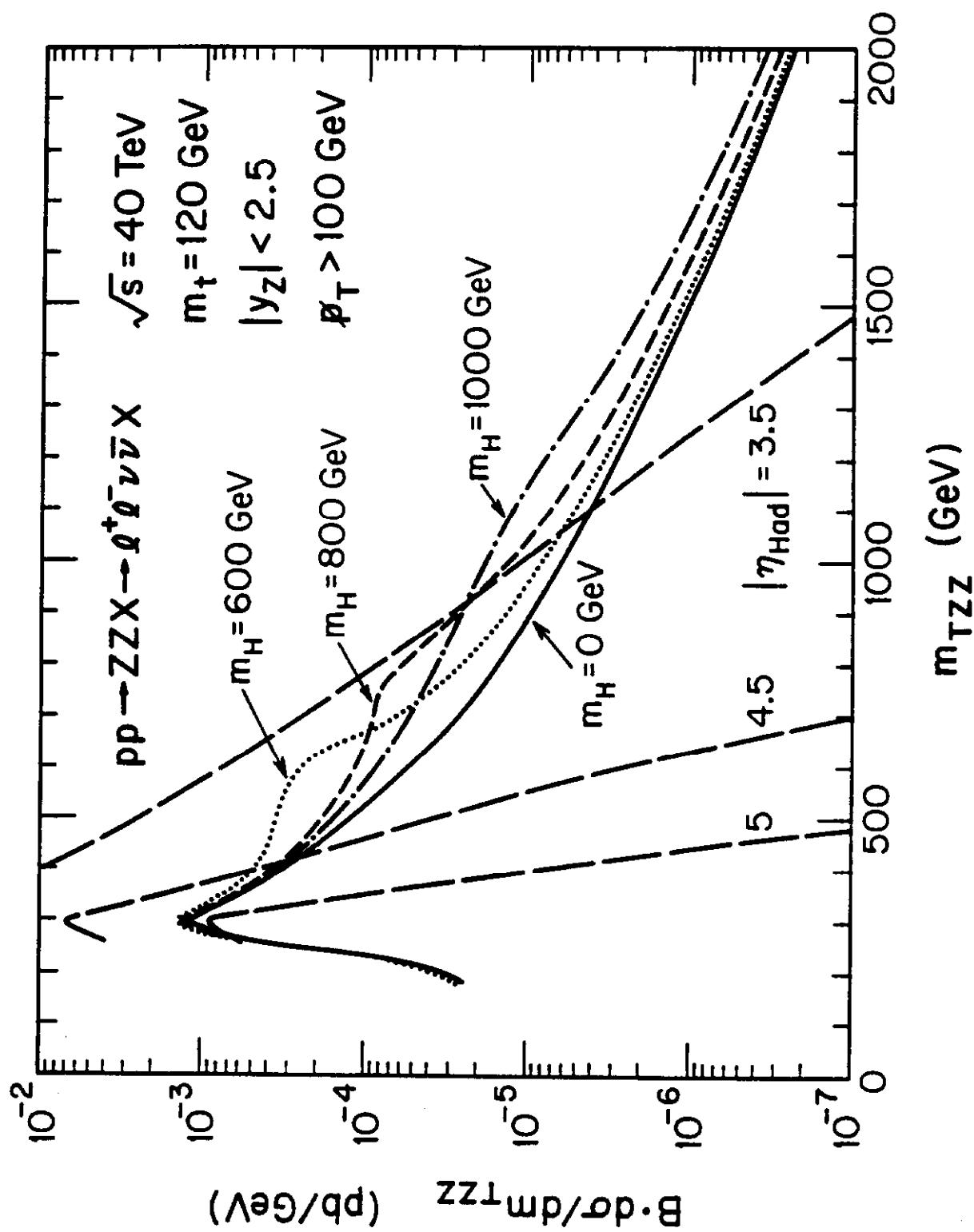


Fig. 4b

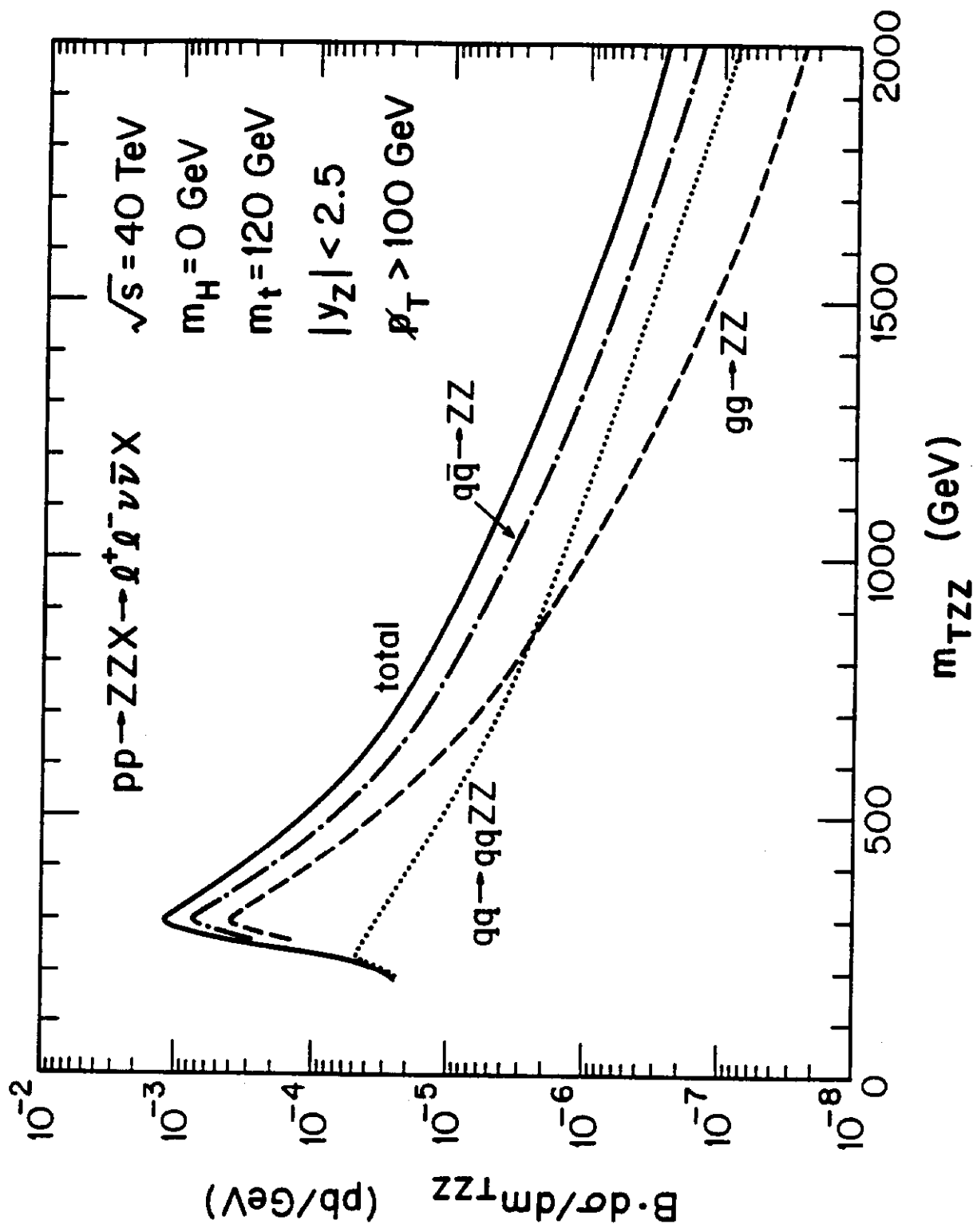


Fig. 5

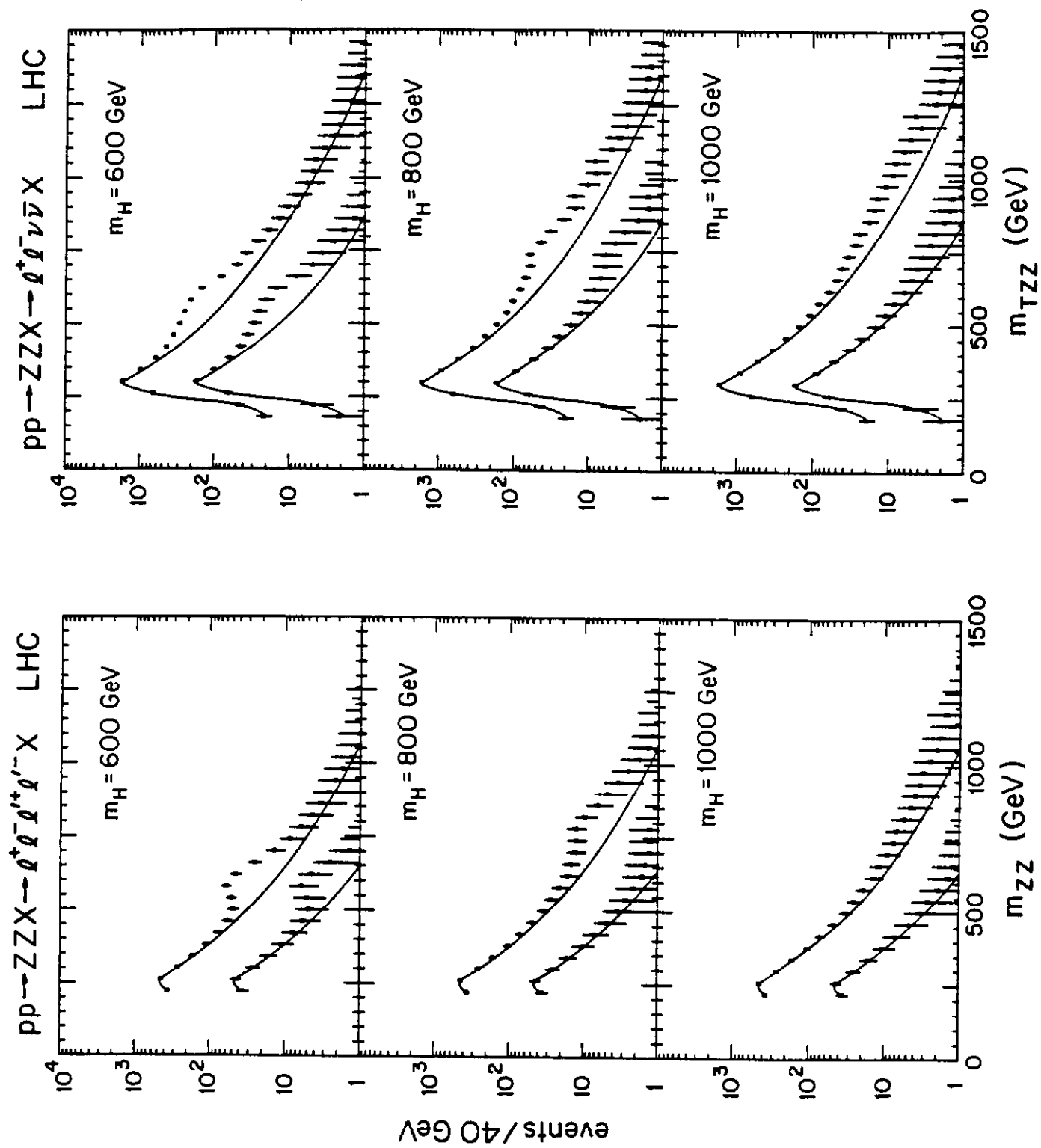


Fig. 6

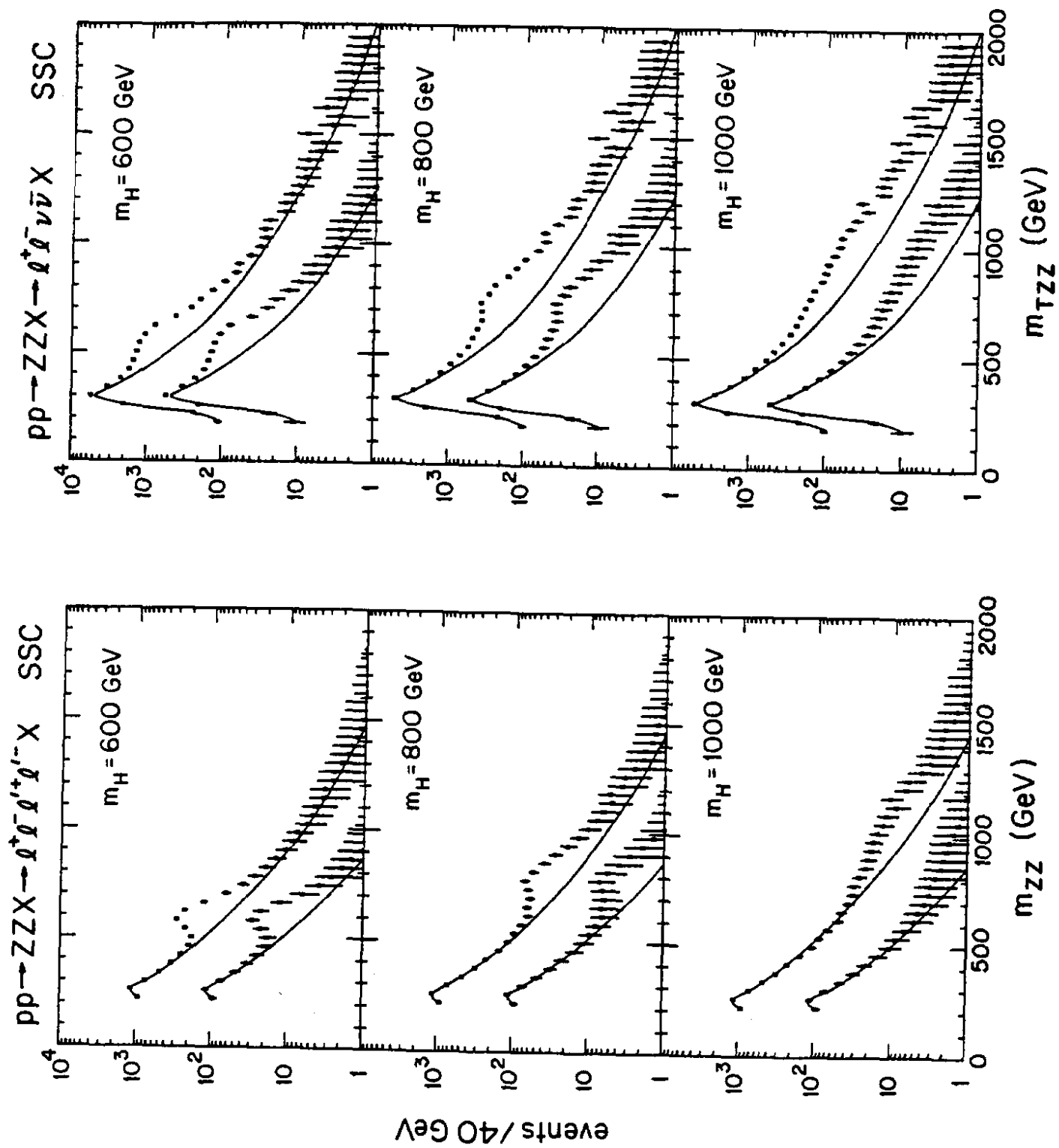


Fig. 7